Hindawi
Advances in Materials Science and Engineering
Volume 2019, Article ID 2896938, 15 pages
https://doi.org/10.1155/2019/2896938

Research Article

Estimation of Inelastic Interstorey Drift for OSB/Gypsum Sheathed Cold-Formed Steel Structures under Collapse Level Earthquakes

Xiangbin Liu, Hanheng Wu, Liurui Sang, Lu Sui, and Congcong Xu

School of Civil Engineering, Chang'an University, Middle-Section of Nan'er Huan Road Xi'an, Shaanxi Province 710061, China

Correspondence should be addressed to Hanheng Wu; wuhanheng@163.com

Received 15 January 2019; Revised 16 May 2019; Accepted 9 June 2019; Published 23 June 2019

Academic Editor: Jun Liu

In order to estimate the inelastic interstorey drift of cold-formed steel (CFS) framed structures under collapse level earthquakes, the deflection amplification factor η_p is employed in this paper to compute the maximum interstorey drift ratio (IDR_{max}) from an elastic analysis. For this purpose, a series of CFS wall specimens were tested under cyclic horizontal loads, and then the hysteresis model of the walls was put forward by test results. In terms of the hysteresis model, a large quantity of elastic-plastic time-history analysis of CFS building structures was conducted based on the storey shear-type model. Furthermore, the deflection amplification factor η_p for estimating IDR_{max} and the parameters were analyzed. The results indicate that the deflection amplification factor η_p is highly dependent on yielding coefficient of storey shear force ξ_y, storey number N, period of structure T, and ground acceleration records GA. Eventually, an approximate ξ_y-N-η_p relationship for estimating the deflection amplification factor η_p is proposed in this paper, which can be used for seismic design in practices.

1. Introduction

In past decades, cold-formed steel (CFS) framed buildings have gained popularity in North America, Europe, Australia, and Japan. In China, cold-formed steel has historically been used for nonstructural members (e.g., curtain walls and partition walls) or secondary structural systems (e.g., purlins and girts), but recently it has also begun to be used as the primary structural members in buildings. Due to their lightweight, environmental friend, low cost, and easy installation, the Chinese government actively promotes CFS framed buildings. Two national technical specifications [1, 2] for low-rise and mid-rise CFS buildings have been officially promulgated. Regretfully, significant researches have been performed on individual CFS members (e.g., CFS studs, walls, purlins, roofs, or floors), but little research has been done on the structural system for CFS buildings. Seismic performance-based design for CFS buildings has also remained out of reach.

It is well known that the interstorey drift ratio (IDR) is defined as the ratio of the relative displacements between two consecutive floors divided by storey height. Actually, IDR is an important parameter in analyzing the seismic response of building structures. In the elastic range, the IDR of structures can be easily obtained by elastic lateral force and elastic stiffness. However, it is difficult to estimate the maximum inelastic displacement in a major earthquake. A correct and convenient evaluation method on maximum nonlinear IDR (IDR_{max}) is fairly significant to seismic analysis and design of buildings. Especially for the modern seismic performance-based design, the IDR_{max} is also required to ensure the limitation of damage and economic losses during frequent earthquakes. However, the effective and practical estimate methods on IDR_{max} for CFS buildings are not involved in current design codes [3–5].

To estimate the IDR_{max} under collapse level earthquakes, the elastic structural analysis together with the deflection amplification factor (DAF) was conventionally employed without resorting to a complex elastoplastic time-history analysis. For traditional RC structures and steel moment framed structures, many research programs concerning DAF have been carried out. Mohammadi [6] clarified the

parameters that have an effect on the DAF and then developed an empirical formula. Lee et al. [7] proposed a simple method on peak interstorey drift for perimeter shear wall structures with flexible or stiff diaphragms. The method considering the shape of design response spectrum can be used for preliminary structural design. Hatzigeorgiou and Beskos [8] presented a simple and effective estimation of IDR_{max} under repeated or multiple earthquakes, and extensive parameters, including vibration period, viscous damping ratio, strain-hardening ratio, force reduction factor, and soil class, were considered in the expressions for the ratio of maximum inelastic displacement to maximum elastic response. Based on the model of shear-flexural beams, Yang et al. [9] investigated the IDR demands of building structures subjected to near-fault ground motions. Caterino et al. [10] put forward two approximate methods on calculating interstorey drift of RC structures, and the methods were proved to be accurate through comparisons between the FEM results and the standard calculation according to the Italian seismic code. d'Aragona et al. [11] developed a simplified assessment of IDR_{max} for RC buildings with irregular distribution of infill panels along the height, and a good agreement between the calculated IDR_{max} and the record processing results was obtained.

In order to develop the seismic performance of CFS structural system, Fiorino et al. [12] carried out the incremental dynamic analysis of one-storey CFS buildings by using the hysteresis response of CFS shear walls. On the research project of CFS-NEES, Schafer et al. [13, 14] conducted a sequential experiment process from small-scale tests on fasteners to full-scale tests on CFS buildings, and their ultimate objective was the advanced simulation tools for CFS framed buildings in terms of seismic performance-based design evaluations. In order to evaluate the seismic response of CFS global buildings, shake table tests on a full-scale two-storey CFS building were carried out by Fiorino et al. [15], and the relevant dynamic identification and earthquake performance were then obtained. Additionally, within the European research project named "ELISSA," Fiorino et al. [16] developed the numerical models of CFS shear walls sheathed with nailed gypsum panels to meet the objectives of performance-based seismic design. Moreover, the hysteretic models of CFS-braced stud walls and the behaviour factor q for systems according to FEMA P695 [17] were also performed by Fiorino and his team [18, 19]. Besides, the dynamic response history analyses and further fragility studies of steel-sheathed CFS framed structures were conducted by Shamim and Rogers [20], and the seismic force modification factors of $R_d = 2$ and $R_o = 1.3$ were proved to be appropriate to the structures in Canada.

In this paper, attention is focused on the estimation of IDR_{max} for traditional OSB/gypsum sheathed CFS framed structures under collapse level earthquakes according to the Chinese seismic code [21]. A series of CFS walls with OSB/gypsum sheathings were tested under cyclic horizontal loads, and then the hysteresis models of the walls were put forward by test results. Based on wall hysteresis models, a large quantity of elastic-plastic time-history analysis of the structures was conducted in accordance with the validated storey shear-type model. Furthermore, the deflection amplification factor (DAF) for estimating IDR_{max} and the parameters were analyzed. A statistical evaluation of DAF was eventually presented, which can be used in the estimation of IDR_{max} for CFS framed structures in practices.

2. Seismic Design Procedure and Deflection Amplification Factor in China

The current seismic design procedure [21] in China includes two steps:

(1) Under design earthquake ground motions (exceedance probability of 10% in 50 years): by using response modification coefficient (R factor), the design earthquake response spectral accelerations are obtained by reduction. The structures are designed within elastic states. Therefore, the elastic design of bearing capacity and deformation is required. It is noted that the interstorey drift limit in elastic stages is 0.33% for CFS framed structures according to the Chinese specifications.

(2) Under collapse level ground motions (exceedance probability of 2% in 50 years): in the step, the structures inevitably show the inelastic manner. Therefore, the collapse of structures is required to be avoided. According to the current Chinese standard, the check of IDR_{max} is needed. To prevent collapse, the interstorey drift limit in inelastic states is taken as 2% for CFS building.

The objective of this paper is to provide an estimation method for IDR_{max} under collapse level ground motions, and the IDR_{max} can be computed from an elastic structural analysis multiplied by the deflection amplification factor η_p, that is,

$$\delta_{max} = \eta_p \delta_e, \tag{1}$$

where δ_{max} is the maximum inelastic interstorey drift, δ_e is the interstorey drift computed from an elastic analysis of structures subjected to the equivalent seismic forces in the collapse level, and η_p is the deflection amplification factor.

3. Cyclic Loading Tests on CFS Shear Walls

A series of cyclic loading tests on CFS shear walls have been successively performed by the research center for cold-formed steel structures at Chang'an University (CFS-CHD). The complete test program is detailed in the CFS-CHD research reports [22–24], and the summary of the results is presented here.

3.1. Test Program. The details of the labeling and descriptions of the full-scale specimens are presented in Table 1. C-section studs and U-section tracks were used to assemble the wall frames. Chord studs were assembled by two C-section studs connected back to back. All specimens with sheathings on one side or both sides were assembled with a height of 3000 mm. The sheathings of the specimens have a

Table 1: Summary of the test matrix.

Name	Wall size	Studs				Sheathing (one side/the other side)
	Width × height (m × m)	Studs ($h \times b \times a \times t$) (mm)	Tracks ($h \times b \times t$) (mm)	Yield stress (MPa)	Spacing (mm)	
BX-A	4 × 3	C89 × 44.5 × 12 × 1.2	U92 × 40 × 1.2	280	500	OSB[a]/gypsum[b]
BX-B	2 × 3					
BX-2A	2.4 × 3	C89 × 44.5 × 12 × 1.0	U92 × 40 × 1.2	320	600	Gypsum[b]/none
BX-2B						
BX-2C						
BX-4A						OSB[a]/none
BX-4B						
BX-4C						
BX-6						OSB[a]/gypsum[b]
BX-7						
BX-8	2.4 × 3.3					Gypsum[b]/none
BX-9						OSB[a]/none
WA-2	2.4 × 3	C140 × 41 × 14 × 1.6	U141 × 34 × 1.6	330	400	OSB[a]/none
WA-4						CSB[b]/none
W-SO75		C75 × 38 × 8 × 0.75	U78 × 43 × 0.75	550	600	OSB[a]/none
W-SF75						CFB[a]/none
W-OP75						OSB[a]/gypsum[b]
HS-90-1		C90 × 40 × 14 × 1.2	U93 × 35 × 1.2	280		OSB[a]/gypsum[b]
HS-140-1		C140 × 40 × 14 × 1.5	U144 × 35 × 1.5			Gypsum[b]/gypsum[b]

[a]9 mm thickness; [b]12 mm thickness; OSB: oriented strand board; gypsum: gypsum plaster board; CSB: calcium silicate board; CFB: cement fiberboard.

product size of 2,440 mm height, which accordingly leads to a horizontal abutted seam at a distance of 560 mm from the bottom of the specimens. Wall frames and sheathings were connected by using self-drilling screws. The screw spacing was 150 mm at the periphery of the walls and 300 mm at the middle. The configuration details of the specimens are shown in Figure 1.

3.2. Test Setup and Procedure. The test setup is shown in Figure 2. The bottom tracks of the walls were fastened to the rigid ground by a rigid beam. The top tracks were also attached to a rigid beam on the top. And the top reaction beam was connected with an actuator mounted on the reaction wall. Then, the lateral loads were applied by the actuator. In addition, a constant axial load during the tests was also applied by the vertical Jack and the distributive girder. To avoid suffering from the additional bending moment, the universal joints along with the sliding devices were used on the top of the specimens. The axial compressive force of 8 kN was firstly performed. According to the Chinese Standard JGJ 227-2011 [1], the lateral displacement-controlled loading procedures were employed, as shown in Figure 3.

3.3. Results. Typical limit states of CFS shear walls under cyclic loads are characterized by failure of screw connections and relative slips at sheathing seams, as shown in Figure 4. Same to the results of other similar tests, the response of CFS shear walls depends on the shearing behaviour of screw connections. Besides, typical hysteretic responses of CFS shear walls are presented in Figure 5. The response of pinching and no-load slipping is clearly obvious owing to the failure mechanism of screw connections, which dominates the nonlinear manner. Using the EEEP model in accordance with the AISI standard [25], the characteristic values of loads and displacements, including initial stiffness K_0, yield load P_y, peak load P_{max}, and ultimate load P_u along with the corresponding drift angles θ_y, θ_{max}, and θ_u, are obtained and listed in Table 2.

4. Hysteretic Parameter Analysis

4.1. Hysteretic Model. The hysteretic characterization of pinching and slipping of CFS shear walls was pursued by the CA4 model as implemented in CANNY [26]. The CA4 model includes the backbone rule, unloading rule, and pinching rule, as shown in Figure 6.

The backbone rule is a quadrilinear skeleton curve with initial nonlinear points (V_c, D_c), (V_c', D_c'), yielding points (V_y, D_y), (V_y', D_y'), and ultimate points (V_u, μD_y), (V_u', $\mu' D_y'$), as shown in Figure 6(a). The significant nonlinear manner of CFS shear walls can be reflected in the quadrilinear skeleton curve. The unloading rule following a new peak displacement (outside unloading) is directed to a target point, as shown in Figure 6(b). The unloading stiffness is given by K_u in the positive side and K_u' in the negative side, that is,

$$\begin{cases} K_u = \dfrac{\theta V_y + V_m}{\left(\theta V_y / K_0\right) + D_m}, \\ K_u' = \dfrac{\theta V_y' + V_m'}{\left(\theta V_y' / K_0\right) + D_m'}, \end{cases} \tag{2}$$

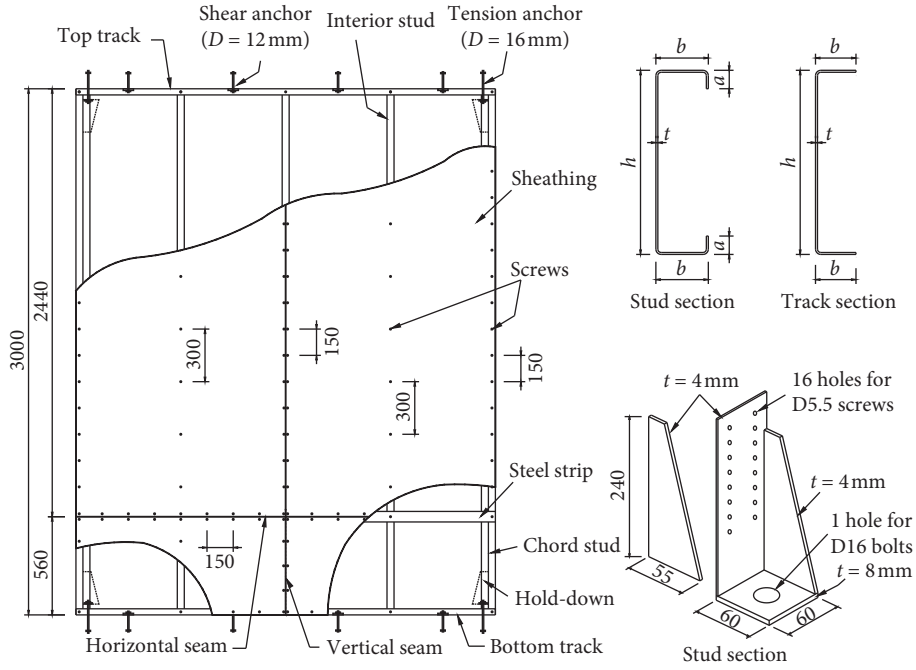

Figure 1: Details of specimen configurations.

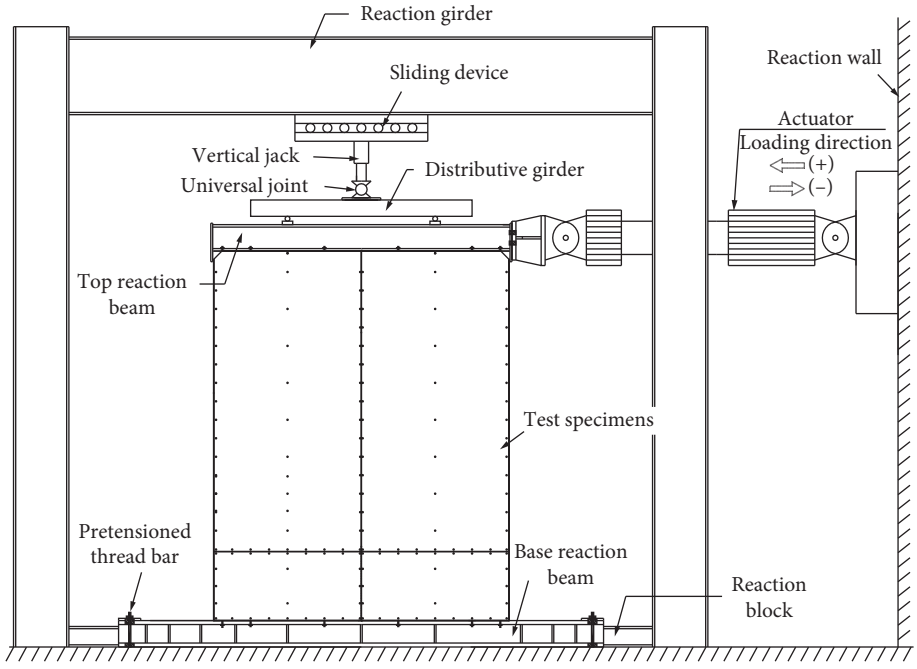

Figure 2: Test setup.

the points (V_m, D_m) and (V'_m, D'_m) are the unloading starting points. The unloading stiffness K_u, K'_u is updated every time when a new peak displacement is reached. The unloading ends at the horizontal axis and follows by reloading towards the opposite direction. The pinching and slipping behaviours of CFS shear walls are mainly caused by the opening and closing of the cracks at screws. Therefore, a target point (V_s, D_s) controlling the slip branch is introduced, as shown in Figure 6(c). For the slip towards positive reloading, the target point is determined as follows:

$$\begin{cases} D_s = D'_0 + \delta\left(D_0 - D'_0\right), \\ V_s = \lambda V_u, \end{cases} \tag{3}$$

and it is the same for the slip towards the negative direction. The zero-crossing displacements D_0 and D'_0 are updated when the unloading occurs from the skeleton curves.

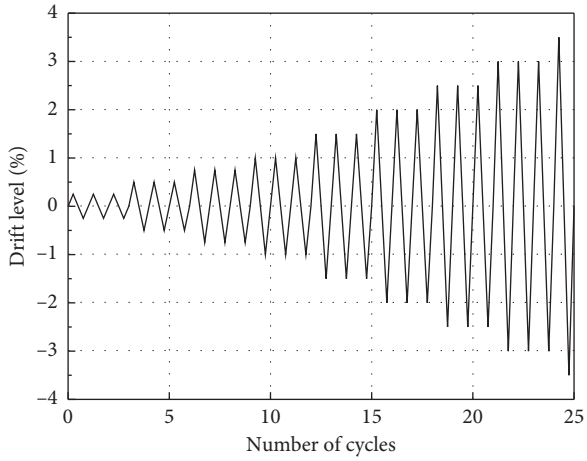

Figure 3: Loading cycles for wall tests.

4.2. Parameter Identification. Referring to the prior discussion, the parameters for the hysteretic model may be classified as the backbone parameters (K_0, V_y, V_u, α, β, γ, and μ), the unloading parameter (θ), and pinching parameters (δ, λ). The tests listed in Table 1 were used to determine the hysteretic parameters, as shown in Table 3. Note that, in this table, the values of K_0, V_y, and V_u have been divided by wall length, so they are the corresponding values per unit length. Besides, it is noted that the initial nonlinear strength V_c, which is not listed in Table 3, is assumed as $0.4V_{max}$ based on the equivalent energy elastic-plastic model (EEEP) in the AISI standard [25].

The resulting hysteresis depends on the selected parameters. As an example of the specimen BX-6, the comparisons of the fitted CA4 model with test data in terms of hysteretic curve and cumulative energy dissipation are provided in Figures 7 and 8, which show a good agreement.

5. Structural Model and Analysis Parameters of CFS Building Structures

5.1. Storey Shear-Type Model. It is well known that CFS shear walls provide lateral resistance for CFS building structures. The shaking table tests [27–29] showed that CFS structures deformed in a manner of shear type under lateral loads. In order to balance the computational efficiency and accuracy, the storey shear-type model, an integrated approach that takes into account the deformation of braced sheathings, sheathing-to-frame connections, hold-downs, and chord studs under shear manner, was employed in this paper (Figure 9). It is noted that the nonrigid diaphragms, the nonstructural components, and the space effect provided by diaphragms and shear walls in longitudinal and transverse directions are neglected in the storey shear-type model. The response of the shear spring in a storey represents the structural behaviour of the storey. The relevant parameters of the shear springs are determined by the sum of CFS walls responses in one direction. Using the hysteretic parameters in Section 4 in this paper, the structural response of the storey can be easily achieved. Besides, the storey mass m_i is concentrated at the level of the n-th storey. The storey shear-type model of such MDOF system is a benchmark for the subsequent dynamic time-history analysis.

5.2. Validations of Storey Shear-Type Model. The shaking table tests introduced in [28] were used to validate the storey shear-type model. According to the experimental details, the dynamic time-history analysis was conducted on the basis of the multistorey shear-type model and the hysteresis rule. Note that the damping ratio is taken as 0.03 conforming to the Chinese Standard JGJ 227-2011 [1]. The comparisons of the fitted model results and test results under the EL-Centro waves are listed in Table 4. The relative error is within an acceptable range of 10%.

5.3. Analysis Parameters. In order to estimate the deflection amplification factor for CFS structures under collapse level earthquakes, a large quantity of dynamic time history analysis was carried out based on the multistorey shear-type model. By using the results of the dynamic analysis, the deflection amplification factor η_p can be easily obtained. Indeed, there are many parameters causing different dynamic analysis results. Therefore, the number of samples for dynamic time history analysis must be sufficient. According to the research results concerning η_p of other structures, the parameters were employed in dynamic time history analysis for CFS structures as follows.

5.3.1. Yielding Coefficient of Storey Shear Force ξ_y. ξ_y is defined as the ratio of the standard shear resistance of CFS shear walls in a storey to the seismic force of the storey computed from an elastic analysis of the structures subjected to collapse level earthquakes. When $\xi_y = 1.0$, it represents that the CFS structures designed are maintained in the elastic condition when suffering from collapse level earthquakes. When $\xi_y = 0$, it represents that the CFS structures have no shear capacity. According to the Chinese anti-collapse design standard [30], when the coefficient ξ_y is smaller than 0.3, the structures are prone to suffering from collapse. Therefore, the coefficient ξ_y should not be smaller than 0.3 ($\xi_y \geq 0.3$). On this account, the yielding coefficient of the storey shear force ξ_y adopted in this paper is 0.3, 0.4, 0.5, 0.6, 0.7, 0.8, 0.9, and 1.0, respectively.

5.3.2. Storey Number N. Two- to seven-storey CFS structures were employed in dynamic time history analysis, which can cover all the low-rise and mid-rise buildings. Besides, the storey height is supposed to be 3 m, which is commonly used in practices.

5.3.3. Period of Structure T. According to the Chinese Standards for CFS structures [1, 2], the fundamental period of the structures can be estimated by the expression $T = (0.02\sim0.03)H$, where H is the height of structures. Three cases of $0.02H$, $0.025H$, and $0.03H$ were accordingly used in this paper.

Figure 4: Typical failure modes of CFS shear walls: (a) failure in gypsum-CFS connections, (b) failure in OSB-CFS connections, and (c) relative slips at board seams.

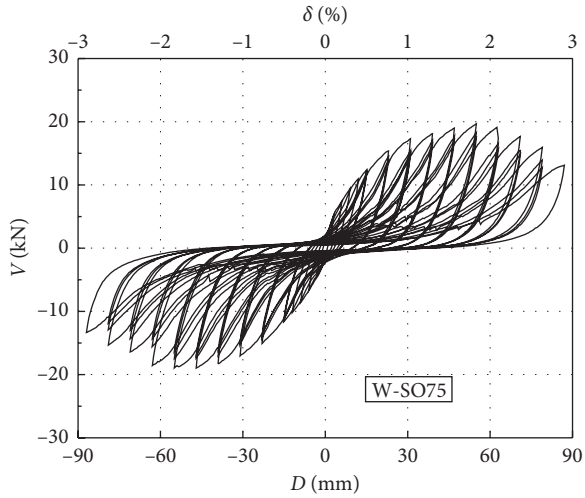

Figure 5: Typical hysteresis curves of CFS shear walls (specimen W-SO75).

5.3.4. Ground Acceleration Records (GA). A total of 20 ground acceleration records were employed in the dynamic time history analysis, which covers the four classifications of the ground site (I, II, III, and IV) illustrated in the Chinese seismic code [21]. The normalized spectral accelerations for four ground sites are shown in Figure 10.

Considering the above parameters, a total of $8 \times 6 \times 3 \times 20 = 2880$ examples (orthogonal design) were calculated by the dynamic time history analysis. Based on these examples, the deflection amplification factor η_p and its influence rule can be captured.

6. Discussion and Analysis of η_p

6.1. Determination of Weak Storey. Under collapse level ground motions, the distribution of inelastic interstorey drift of each storey is nonuniform. The plastic deformation is mainly concentrated in a storey, defined as the weak storey. Correspondingly, the other storeys have a comparatively small or no plastic lateral displacement. According to the concept of energy consumption, the hysteretic energy is also mainly dissipated in the weak storey.

In this paper, the parameter ρ, which is used to evaluate the distribution of hysteretic energy along the height of CFS structures, is introduced as follows:

$$\rho_i = \frac{E_{Hi}}{\sum_{i=1}^{n} E_{Hi}}, \tag{4}$$

where ρ_i is the hysteretic energy ratio of the i-th storey and E_{Hi} is the hysteretic energy dissipation of the i-th storey. Based on the analysis results of the 2,880 examples, the typical distribution rules of the hysteretic energy ratio ρ for CFS structures are illustrated in Figure 11.

Observing Figure 11, the hysteretic energy is mainly dissipated in the first storey. It decreases from ground storey to top storey gradually. Consequently, the first storey is not just the weak storey but the storey where the plastic lateral displacement is concentrated. It is noted that the above conclusions are based on the 2,880 models of CFS structures with the uniform distribution of lateral stiffness and mass. The deflection amplification factor η_p for the first storey (weak storey) is discussed in the following analysis.

6.2. Influence of Yielding Coefficient of Storey Shear Force ξ_y. Due to the huge amount of analysis data, the selected curves of ξ_y vs. η_p are presented in Figure 12. The results show that deflection amplification factor η_p gradually increases with the decreasing yielding coefficient ξ_y. This rule is also confirmed by the analysis models with different storey number N and different GA in Section 5 of this paper. For the reason that ξ_y is defined as the ratio of shear capacity of a storey to the seismic shear force by elastic analysis, the storey shear capacity gradually decrease with the coefficient ξ_y from 1.0 to 0.3 and the weak storey accordingly reach to the state of plasticity earlier. Therefore, the CFS structures with the smaller ξ_y presented the larger plastic deformation.

Table 2: Experimental results.

Name	K_0 (kN/m)	P_y (kN)	θ_y (rad) (%)	P_{max} (kN)	θ_{max} (rad) (%)	P_u (kN)	θ_u (rad) (%)	μ
BX-A	3472	39.04	0.45	46.94	1.33	39.90	2.26	3.83
BX-B	2172	21.74	0.33	25.38	0.73	21.57	1.99	3.45
BX-2A	570	7.35	0.61	8.58	1.25	7.29	2.68	4.38
BX-2B	750	7.65	0.49	9.08	1.40	7.72	2.30	5.00
BX-2C	645	7.72	0.52	8.88	1.23	7.55	2.77	5.32
BX-4A	1650	20.30	0.57	24.50	1.33	20.83	2.09	3.67
BX-4B	1603	19.50	0.56	23.16	1.19	19.69	2.08	3.74
BX-4C	1720	21.00	0.59	25.59	1.18	21.75	2.03	3.42
BX-6	2040	24.20	0.55	27.95	1.60	23.76	2.06	3.75
BX-7	2560	25.40	0.65	30.52	0.92	25.94	1.87	4.01
BX-8	713	7.80	0.51	9.00	1.23	7.65	2.61	5.15
BX-9	1680	20.8	0.57	25.17	0.83	21.39	2.11	3.72
WA-2	3274	22.15	0.84	29.69	1.33	25.24	2.67	3.18
WA-4	3569	32.83	0.41	37.31	0.59	31.71	1.01	2.45
W-SO75	1470	16.55	0.51	19.68	1.17	16.73	1.88	3.68
W-SF75	912	10.35	0.41	12.06	0.94	10.25	1.30	3.18
W-OP75	2278	25.44	0.44	30.18	1.16	25.65	1.81	4.07
HS-90-1	3470	28.88	0.42	36.12	1.45	30.70	2.22	5.36
HS-140-1	3864	19.44	0.40	23.62	0.92	20.95	2.27	5.60

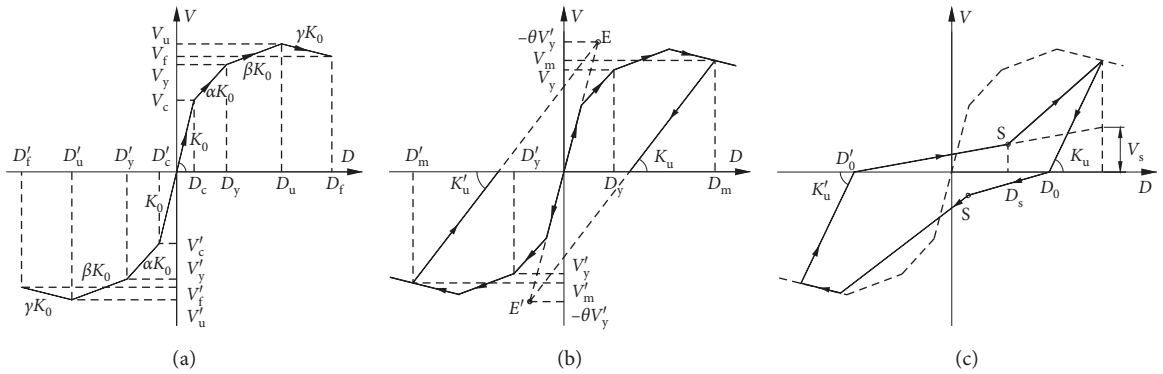

Figure 6: Hysteretic model: (a) backbone rule, (b) unloading rule, and (c) pinching rule.

Table 3: Hysteretic parameters of specimens.

Name	Backbone parameters							Unloading parameter	Pinching parameters	
	K_0 (kN·m^{-2})	V_y (kN·m^{-1})	V_u (kN·m^{-1})	α	β	γ	μ	θ	δ	λ
BX-A	868.0	9.76	11.74	0.199	0.061	−0.062	3.83	10.2	0.82	0.25
BX-B	1086.0	10.87	12.69	0.261	0.075	−0.046	3.45	8.9	0.69	0.19
BX-2A	237.5	3.06	3.58	0.219	0.071	−0.034	4.38	11.4	0.73	0.20
BX-2B	312.5	3.19	3.78	0.256	0.058	−0.039	5.00	10.7	0.75	0.14
BX-2C	268.8	3.22	3.70	0.392	0.053	−0.029	5.32	9.1	1.01	0.30
BX-4A	687.5	8.44	10.21	0.331	0.088	−0.082	3.67	8.9	0.94	0.14
BX-4B	668.3	8.13	9.65	0.286	0.085	−0.064	3.74	9.9	0.89	0.17
BX-4C	716.7	8.75	10.66	0.365	0.102	−0.073	3.42	12.3	0.71	0.23
BX-6	850.0	10.08	11.65	0.317	0.074	−0.103	3.75	7.5	0.99	0.33
BX-7	1066.7	10.58	12.72	0.292	0.083	−0.065	4.01	9.1	0.84	0.09
BX-8	297.1	3.25	3.75	0.314	0.099	−0.087	5.15	10.0	0.85	0.15
BX-9	700.0	8.67	10.49	0.287	0.071	−0.098	3.72	9.4	0.77	0.19
WA-2	1364.4	9.23	12.37	0.301	0.103	−0.069	3.06	13.6	1.03	0.27
WA-4	1487.1	13.68	15.55	0.246	0.079	−0.112	2.49	11.7	1.15	0.26
W-SO75	612.5	6.90	8.20	0.308	0.057	−0.107	3.68	9.6	0.77	0.17
W-SF75	380.4	4.31	5.03	0.225	0.081	−0.079	3.18	9.3	0.98	0.30
W-OP75	949.2	10.60	12.58	0.347	0.076	−0.086	4.07	7.8	0.87	0.28
HS-90-1	1446	12.03	15.05	0.370	0.072	−0.057	5.36	10.4	0.90	0.17
HS-140-1	1610	8.10	9.85	0.299	0.069	−0.034	5.33	9.2	1.04	0.20
Average value	n.a.	n.a.	n.a.	0.296	0.077	−0.070	4.03	9.9	0.88	0.21

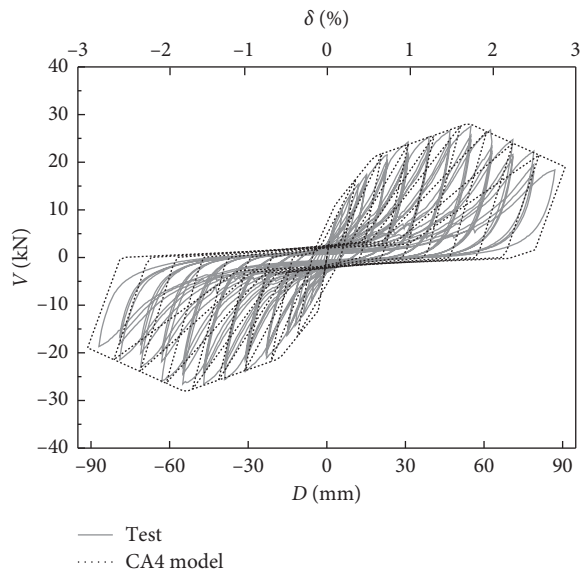

Figure 7: Comparison of test V-D response with fitted CA4 model.

6.3. Influence of Storey Number N. The analysis reveals that the impact of storey number N to the deflection amplification factor η_p is apparent. With the increase in storey number N, the deflection amplification factor η_p accordingly increases. The typical curves of the influence of storey number N are presented in Figure 13.

6.4. Influence of Structural Period T. The fundamental period of structures can affect the deflection amplification factor η_p; however, the influence rules are not clear, which vary greatly depending on the different cases (e.g., ξ_y, N, and GA). The selected curves in regard to the vague influence of structural period T are shown in Figure 14.

6.5. Influence of Ground Acceleration Records (GA). Compared with the η_p under the other three ground sites (Figure 15), the deflection amplification factor η_p of the examples is relatively large when they subject to the ground acceleration records of site IV. The reason is that the structural period of CFS structures is commonly less than 0.65 s ($T \le 0.65$ s), but in general, the characteristic period T_g of ground site IV is greater than 0.65 s ($T_g \ge 0.65$ s). The case of $T \le T_g$ results in a larger displacement response.

7. Practical Method on the Estimation of η_p

Based on the 2,880 examples, it is shown that the deflection amplification factor η_p is highly dependent on the parameters ξ_y, N, T, and GA. The influence rules of the parameters ξ_y and N on the factor η_p are clear; however, it must be noted that the considering parameters T and GA do not affect the factor η_p significantly and clearly.

With the above in mind, an approximate ξ_y-N-η_p relationship for estimating the deflection amplification factor η_p is employed in this paper for practices, while the influence of parameters T and GA can be eliminated by the statistical method. Finally, the average of data plus 1.645 times of the variances is used, which can provide 95% of assurance rate. The employed ξ_y-N-η_p relationship is shown in Table 5 and Figure 16, and then by using equation (1), the maximum inelastic interstorey drift under collapse level earthquakes can be easily calculated.

8. Discussion of η_p

The deflection amplification factor η_p in this paper is different from the factor C_d introduced in FEMA 695 [17]. Indeed, $\eta_p = C_d/R$, as follows.

The response modification factor (R) is commonly expressed in terms of two main components: the ductility reduction factor (R_μ) and the structural overstrength factor (Ω_0). The R factor is defined as

$$R = R_\mu \times \Omega_0 = \frac{V_e}{V_y} \times \frac{V_y}{V_d} = \frac{V_e}{V_d}. \tag{5}$$

The deflection amplification factor (C_d) can be expressed by the following formula:

$$C_d = \frac{\delta_{max}}{\delta_d} = \frac{\delta_{max}}{\delta_e} \times \frac{\delta_e}{\delta_d}. \tag{6}$$

According to the linear relation, V_e/V_d is equal to δ_e/δ_d, as follows:

$$\frac{V_e}{V_d} = \frac{\delta_e}{\delta_d}. \tag{7}$$

By substituting equations (5) and (7) into equation (6), the expression for C_d can be derived:

$$C_d = \frac{\delta_{max}}{\delta_e} \times R. \tag{8}$$

However, the deflection amplification factor η_p in this paper is defined as the ratio of δ_{max} to δ_e, as follows:

$$\eta_p = \frac{\delta_{max}}{\delta_e}. \tag{9}$$

Substituting equation (9) into equation (8), the relationship of η_p, R, and C_d can be expressed as

$$\eta_p = \frac{C_d}{R}. \tag{10}$$

Based on the classical "Newmark rule," the value of C_d is equal to the value of R ($\eta_p = 1$), which assumes that inelastic displacement is approximately equal to elastic displacement. According to the FEMA P695, this is consistent with research findings for systems with nominal (5% of critical) damping and fundamental periods greater than the transition period, T_s. But for short-period systems ($T < T_s$), inelastic displacement generally exceeds elastic displacement. Therefore, it is not considered appropriate to the deflection amplification factor on response of short-period systems. According to the related studies [6, 31, 32], the ratio of C_d to R ($\eta_p = C_d/R$ in this paper) is dependent on the structural ductility μ and fundamental period T.

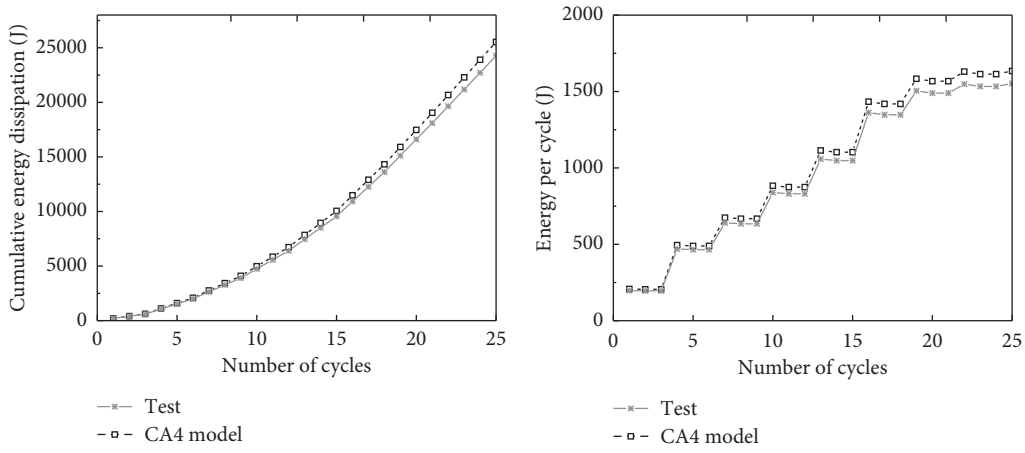

Figure 8: Comparison of experimental and numerical results: (a) cumulative energy dissipation and (b) energy per cycles.

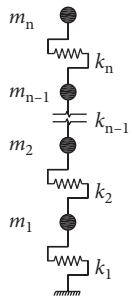

Figure 9: Structural model selected for dynamic analysis.

Table 4: Comparisons of model results and test results.

Item	Fundamental period (s)	Base shear (kN)	Top acceleration (gal)	Maximum interstorey drift ratio
TEST	0.198	25.75	1154	0.56%
Numerical model	0.216	23.61	1085	0.51%
Error	9.09%	8.31%	5.95	9.52%
Notes	White noise signal	Design level	Collapse level	Collapse level

Through data fitting, the ξ_y-N-η_p relationship introduced in Part 7 can be expressed as

$$\eta_p = -0.012N^{2.55} \cdot \ln \xi_y + 1.27, \tag{11}$$

and the comparison of the fitting equation (11) with the ξ_y-N-η_p relationship in Figure 16 (or Table 5) is presented in Figure 18, which shows a good agreement.

With regard to the yielding coefficient of storey shear force ξ_y, defined as the ratio of shear capacity to the seismic shear force by elastic analysis, indeed, it is the ratio of V_y to V_e, as shown in Figure 17. It can be found that the coefficient ξ_y and ductility reduction factor R_μ are reciprocal, as follows:

$$\xi_y = \frac{V_y}{V_e} = \frac{1}{R_\mu}, \tag{12}$$

and the classical ductility reduction rule proposed by Newmark and Hall for a SDOF system can be used:

$$R_\mu = \begin{cases} \mu, & \text{for} \quad T \geq T_s, \\ \sqrt{2\mu - 1}, & \text{for} \quad T < T_s. \end{cases} \tag{13}$$

For the low-rise and mid-rise CFS structures, the fundamental period T is usually smaller than the transition period T_s on account of the relationship of period T and structural height H ($T = (0.02\sim0.03)H$). Taking seven-storey CFS structures, for example (storey height is supposed to be 3 m), its fundamental period T is about 0.42 s–0.63 s. Accordingly, the low-rise and mid-rise CFS structures are short-period systems and the R_μ-μ relationship for $T < T_s$ is appropriate. Taking the median, the fundamental period T is taken as $0.025H$. The storey height is still assumed to be 3 m, and the relationship of fundamental period T and storey number N can be accordingly expressed as

$$T = 0.075N. \tag{14}$$

Then by substituting $T = 0.075N$ together with equations (12) and (13) into equation (11), the ξ_y-N-η_p relationship can be transformed into the relationship of μ-T-η_p, as follows:

$$\eta_p = 8.87T^{2.55} \cdot \ln\left(\sqrt{2\mu - 1}\right) + 1.27, \tag{15}$$

and the impact of ductility μ and period T on the deflection amplification factor η_p can be described by equation (15) in quantitative terms.

In fact, the relationship of μ-T-η_p is widely discussed for other structural systems. Hwang and Jaw [31] proposed the following expression to determine the DF (same to η_p in this paper) for MDOF reinforced concrete buildings:

$$\text{DF} = \mu^{0.414}. \tag{16}$$

Obviously, the factor of period T is neglected in the expression. Baez and Miranda [32] and Mohammadi [6] have suggested the expressions for μ-T-DF (or μ-T-η_p) relationship, as follows:

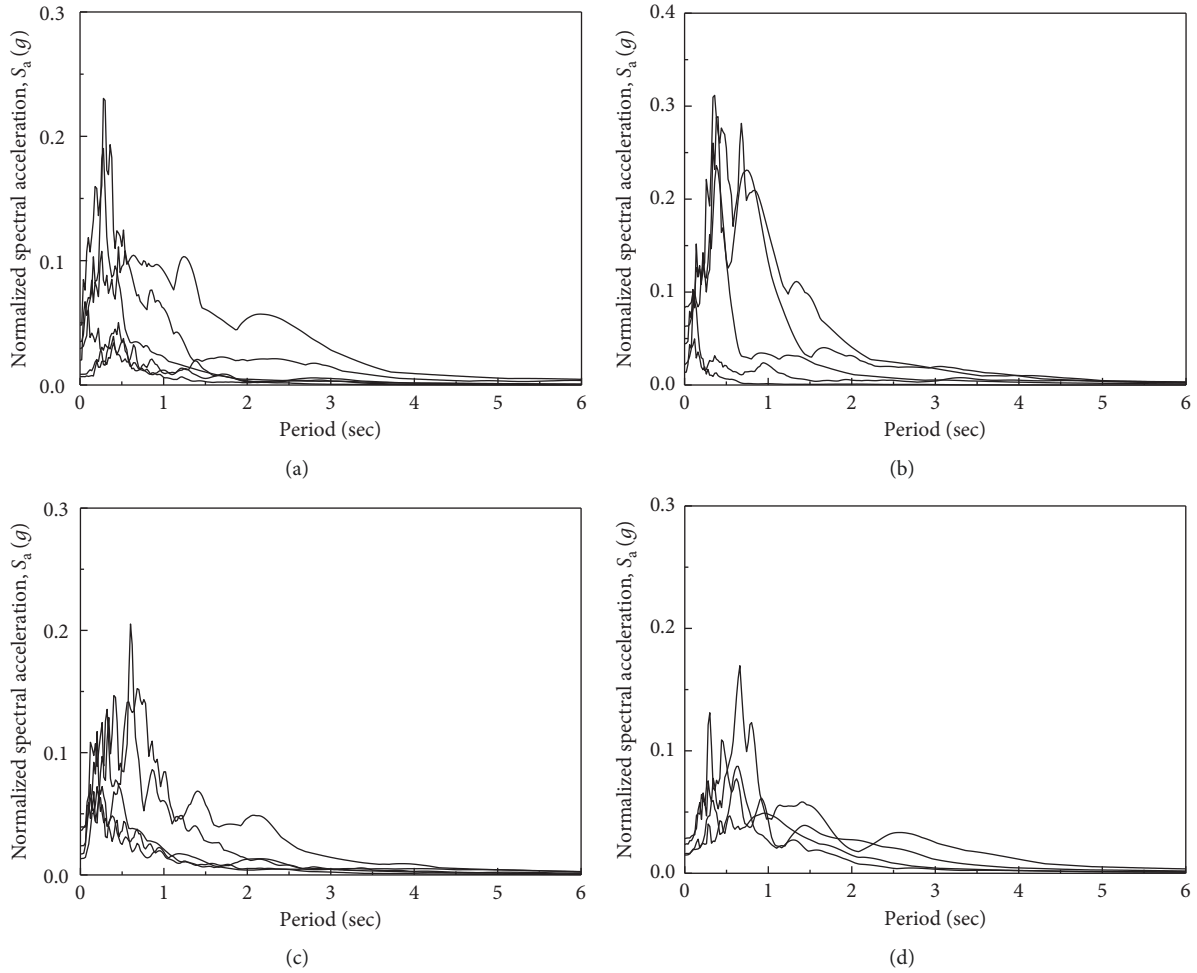

Figure 10: Normalized spectral acceleration for four ground sites. (a) Ground site, I (b) ground site II, (c) ground site III, and (d) ground site IV.

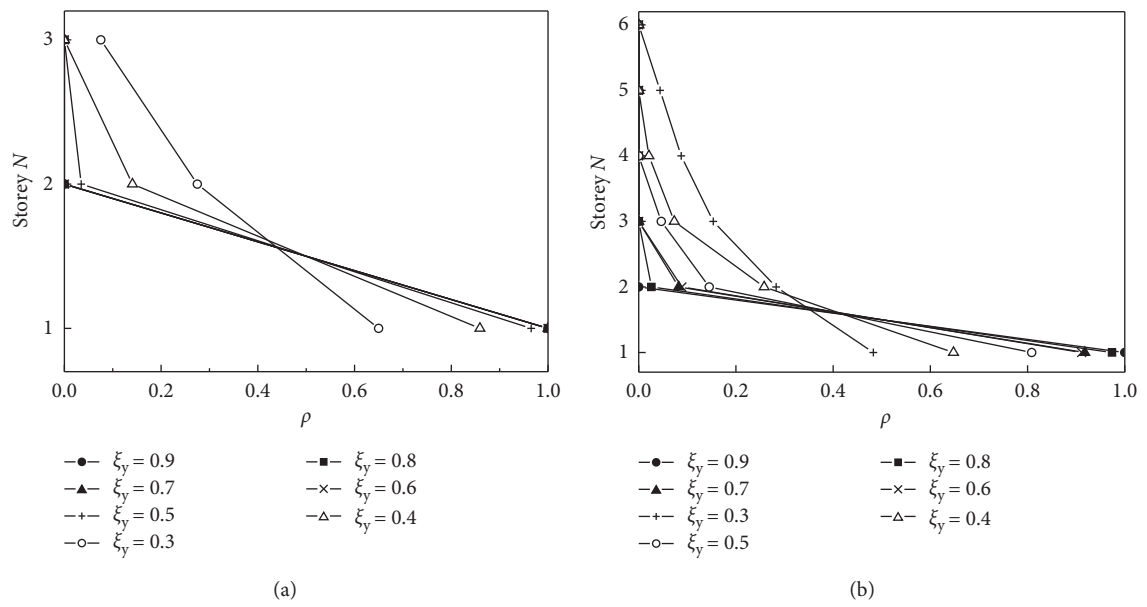

Figure 11: Hysteretic energy ratio ρ_i: (a) 3-storey structure, $T = 0.18$ s, Loma Prieta waves and (b) 6-storey structure, $T = 0.45$ s, San Fernando waves.

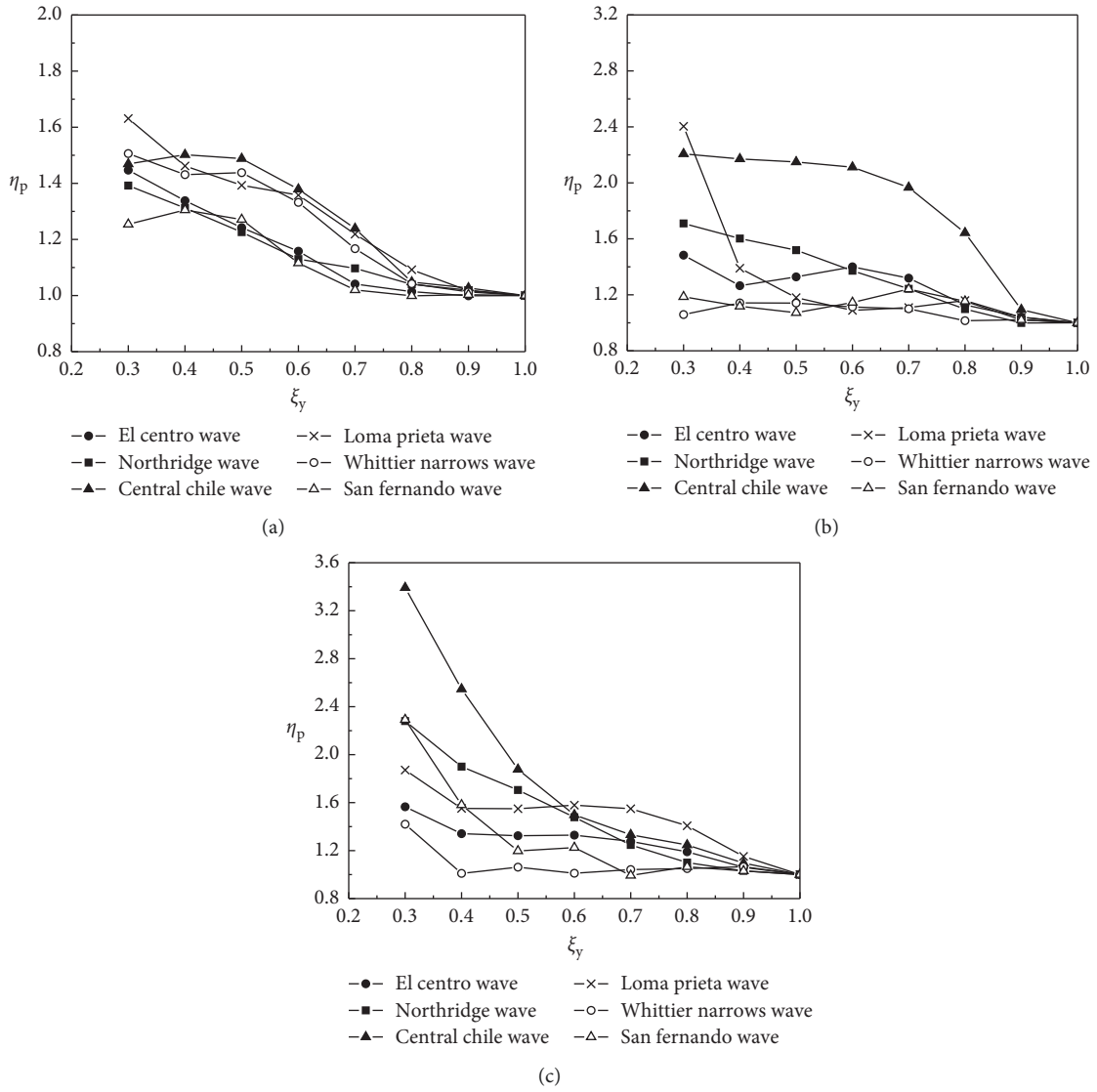

Figure 12: Influence of yielding coefficient of storey shear force ξ_y: (a) 3-storey structure ($T = 0.225$ s), (b) 5-storey structure ($T = 0.375$ s), and (c) 6-storey structure ($T = 0.45$ s).

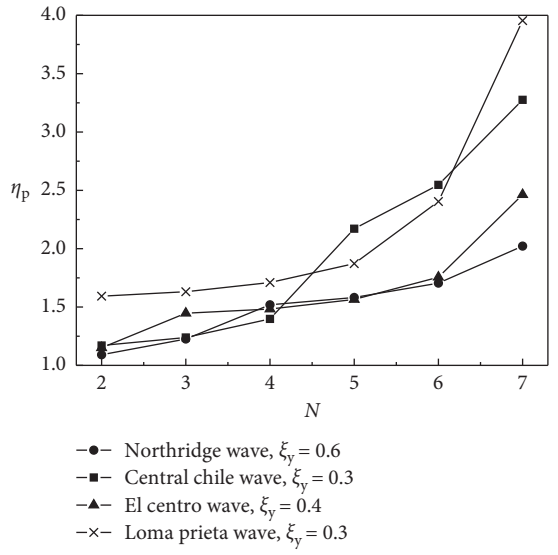

Figure 13: Influence of storey number N.

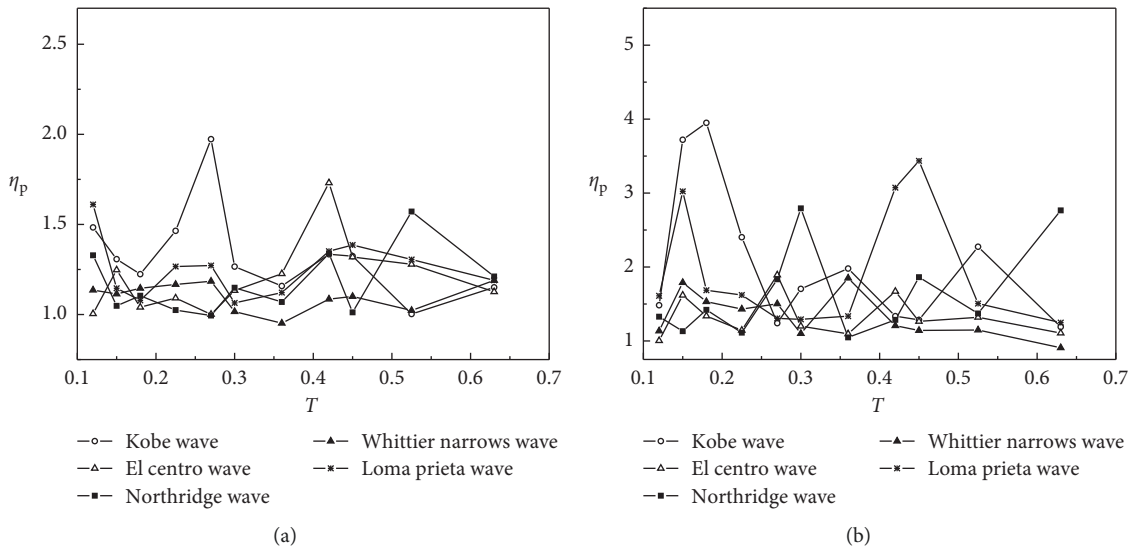

Figure 14: Influence of structural period T: (a) $\xi_y = 0.7$ and (b) $\xi_y = 0.4$.

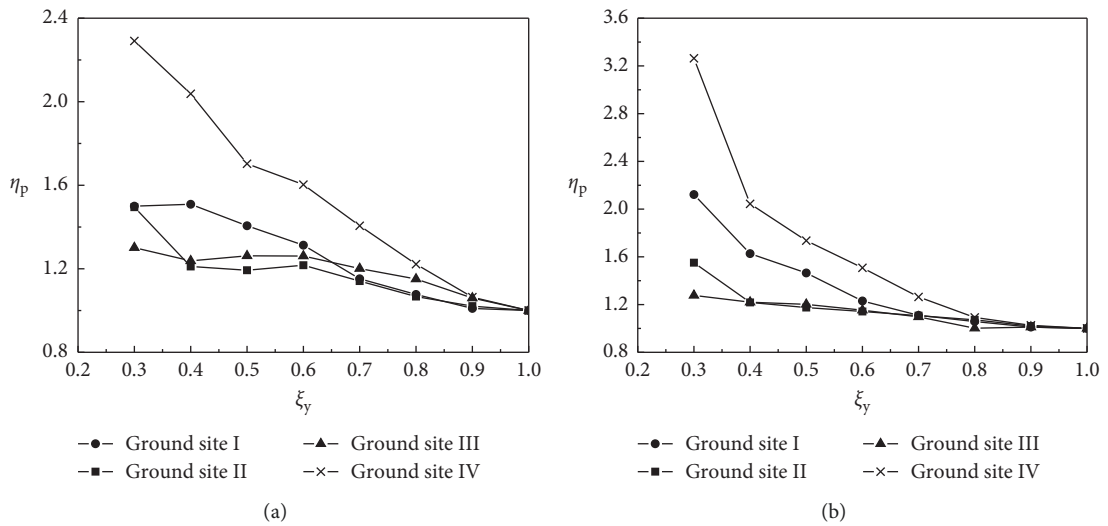

Figure 15: Influence of ground acceleration records (GA): (a) 5-storey structure ($T = 0.30$ s) and (b) 6-storey structure ($T = 0.36$ s).

Table 5: Estimated values of η_p for seismic design.

Storey number N	Yielding coefficient of storey shear force ξ_y					
	0.8	0.7	0.6	0.5	0.4	0.3
2	1.30	1.31	1.32	1.33	1.34	1.38
3	1.33	1.35	1.38	1.42	1.47	1.55
4	1.38	1.42	1.48	1.53	1.61	1.80
5	1.43	1.49	1.61	1.68	1.80	2.13
6	1.50	1.59	1.78	1.86	2.06	2.64
7	1.59	1.71	2.03	2.15	2.46	3.46

$$\mathrm{DF} = \frac{1}{1 + ((1/\mu) - 1)\exp\left(-12T\mu^{-0.8}\right)}, \tag{17}$$

$$\mathrm{DF} = (0.78 + 0.17\mu) \cdot n^{(0.27-0.004n)} + (0.03 - 0.24\mu) \cdot T, \quad T \le 0.8\mathrm{s}. \tag{18}$$

Comparisons of different DFs (or η_p) suggested by equations (15)–(18) with various ductility demands are depicted in Figure 19. It is clear that the deflection amplification factor increases gradually with the increase in structural ductility. However, the influence rule of structural period is still uncertain, and different studies show different results.

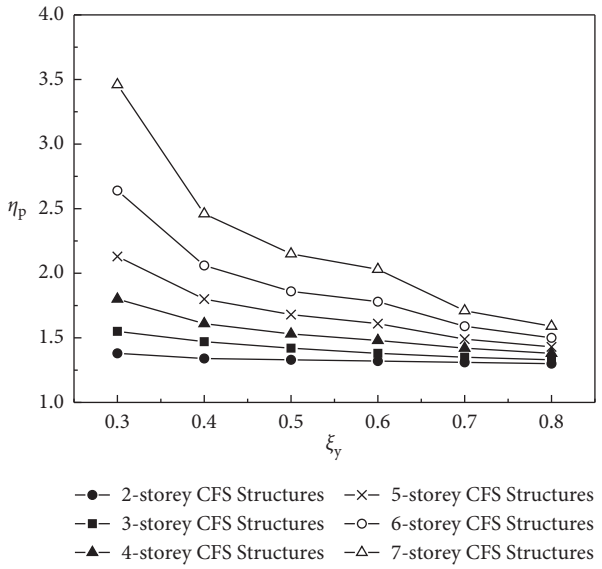

Figure 16: Suggested ξ_y-N-η_p relationship for seismic design.

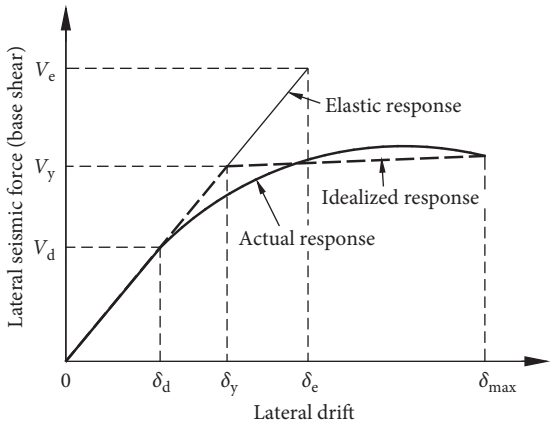

Figure 17: Illustration of seismic performance factors.

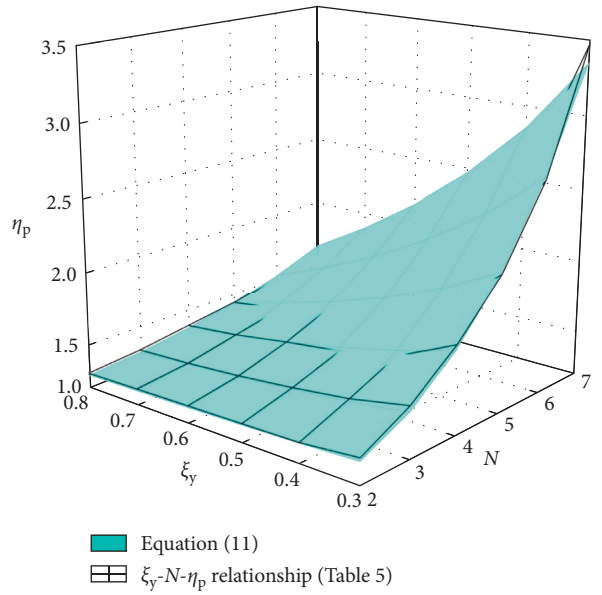

Figure 18: Comparison of the fitting equation (11) with the suggested ξ_y-N-η_p relationship.

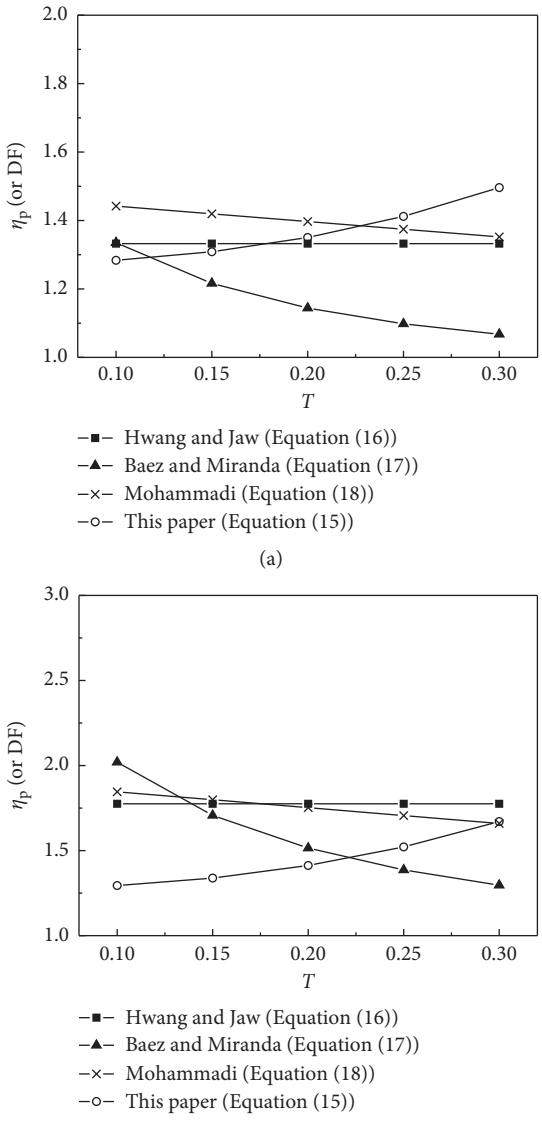

Figure 19: Comparison between different suggested values of deflection amplification factor for 3-storey model ($T = 0.02 \sim 0.03$) H: (a) $\mu = 2.0$ and (b) $\mu = 4.0$.

9. Conclusions and Recommendations

The hysteresis models and parameters of CFS shear walls were proposed in this paper. According to the multistorey shear-type model, 2880 examples of CFS structures were conducted by elastoplastic time-history analysis. Based on the results of the investigation, the following conclusions can be drawn:

(1) The hysteretic responses of CFS shear walls are characterized by the phenomenon of pinching and no-load slipping, which is mainly caused by the nonlinear manner of screw connections. The suggested CA4 hysteretic model is capable of describing the nonlinear features.

(2) It is shown that the deflection amplification factor η_p is mainly dependent on the parameters ξ_y, N, T, and GA. Specifically, with the decreasing yielding coefficient of storey shear force ξ_y and the increasing storey number N, the deflection amplification factor η_p increases gradually. Besides, the factor η_p is relatively large under the ground motions of site IV.

(3) Based on 2880 examples, the approximate ξ_y-N-η_p relationship for estimating the deflection amplification factor η_p is put forward in this paper for design. By using equation (1), the maximum inelastic interstorey drift ratio (IDR_{max}) of CFS structures under collapse level earthquakes can be obtained.

Data Availability

The data used to support the findings of this study are included within the article.

Additional Points

Highlights. The estimation of IDR_{max} for CFS framed structures under collapse level earthquakes is studied. Cyclic loading tests are conducted on CFS walls. The deflection amplification factor for estimating IDR_{max} and the parameters were analyzed. A statistical evaluation of deflection amplification factor is presented, which can be used in IDR_{max} estimation for CFS framed structures in practices.

Disclosure

Any opinions, findings, conclusions, and recommendations expressed in this paper are those of the authors and do not necessarily reflect the views of the sponsors.

Conflicts of Interest

The authors declare that there are no conflicts of interest.

Acknowledgments

This research was financially supported by the Natural Science Foundation of China (No. 51508029), which is gratefully acknowledged. The authors would especially like to thank Chenglong Wang (master) for his contribution to the experimental research.

References

[1] Ministry of Housing and Urban-Rural Development of China, *Technical Specification for Low-Rise Cold-Formed Thin-Walled Steel Buildings, JGJ 227-2011*, Ministry of Housing and Urban-Rural Development, Beijing, China, 2011, in Chinese.

[2] Ministry of Housing and Urban-Rural Development of China, *Technical Standard for Cold-Formed Thin-Walled Steel Multi-Storey Residential Buildings, JGJ/T 421-2018*, Ministry of Housing and Urban-Rural Development, Beijing, China, 2018, in Chinese.

[3] American Iron and Steel Institute (AISI), *North American Standard for Cold-Formed Steel Structural Framing, AISI S240*, American Iron and Steel Institute (AISI), Washington, DC, USA, 2014.

[4] American Iron and Steel Institute (AISI), *North American Standard for Seismic Design of Cold-Formed Steel Structural Systems, AISI S400*, American Iron and Steel Institute (AISI), Washington, DC, USA, 2014.

[5] Australian Institute of Steel Construction, *Cold-Formed Steel Structures, Australian and New Zealand standards, AS/NZS 4600*, Australian Institute of Steel Construction, Sydney, Australia, 2005.

[6] R. K. Mohammadi, "Approximate evaluation of deflection amplification factor," *Journal of Structural Engineering*, vol. 128, no. 2, pp. 179–187, 2002.

[7] H. J. Lee, M. A. Aschheim, and D. Kuchma, "Interstory drift estimates for low-rise flexible diaphragm structures," *Engineering Structures*, vol. 29, no. 7, pp. 1375–1397, 2007.

[8] G. D. Hatzigeorgiou and D. E. Beskos, "Inelastic displacement ratios for SDOF structures subjected to repeated earthquakes," *Engineering Structures*, vol. 31, no. 11, pp. 2744–2755, 2009.

[9] D. Yang, J. Pan, and G. Li, "Interstory drift ratio of building structures subjected to near-fault ground motions based on generalized drift spectral analysis," *Soil Dynamics and Earthquake Engineering*, vol. 30, no. 11, pp. 1182–1197, 2010.

[10] N. Caterino, E. Cosenza, and B. M. Azmoodeh, "Approximate methods to evaluate storey stiffness and interstory drift of RC buildings in seismic area," *Structural Engineering and Mechanics*, vol. 46, no. 2, pp. 245–267, 2013.

[11] M. G. d'Aragona, M. Polese, and E. C. A. Prota, "Simplified assessment of maximum interstory drift for RC buildings with irregular infills distribution along the height," *Bulletin of Earthquake Engineering*, vol. 17, no. 2, pp. 707–736, 2018.

[12] L. Fiorino, O. Iuorio, and R. Landolfo, "Seismic analysis of sheathing-braced cold-formed steel structures," *Engineering Structures*, vol. 34, pp. 538–547, 2012.

[13] B. W. Schafer, D. Ayhan, J. Leng et al., "Seismic response and engineering of cold-formed steel framed buildings," *Structures*, vol. 8, pp. 197–212, 2016.

[14] J. Leng, B. W. Schafer, and S. G. Buonopane, "Modeling the seismic response of cold-formed steel framed buildings: model development for the CFS-NEES building," in *Proceedings of the annual stability conference structural stability research council*, St. Louis, MO, USA, April 2013.

[15] L. Fiorino, V. Macillo, and R. Landolfo, "Shake table tests of a full-scale two-story sheathing-braced cold-formed steel building," *Engineering Structures*, vol. 151, pp. 633–647, 2017.

[16] L. Fiorino, S. Shakeel, V. Macillo, and R. Landolfo, "Seismic response of CFS shear walls sheathed with nailed gypsum panels: numerical modelling," *Thin-Walled Structures*, vol. 122, pp. 359–370, 2018.

[17] Federal Emergency Management Agency (FEMA), *Quantification of Building Seismic Performance Factors, FEMAP695*, Federal Emergency Management Agency (FEMA), Washington, DC, USA, 2009.

[18] V. Macillo, S. Shakeel, L. Fiorino, and R. Landolfo, "Development and calibration of a hysteretic model for CFS strap braced stud walls," *Advanced Steel Construction*, vol. 14, no. 3, pp. 337–360, 2018.

[19] L. Fiorino, S. Shakeel, V. Macillo, and R. Landolfo, "Behaviour factor (q) evaluation the CFS braced structures according to FEMA P695," *Journal of Constructional Steel Research*, vol. 138, pp. 324–339, 2017.

[20] I. Shamim and C. A. Rogers, "Numerical evaluation: AISI S400 steel-sheathed CFS framed shear wall seismic design method," *Thin-Walled Structures*, vol. 95, pp. 48–59, 2015.

[21] Ministry of Housing and Urban-Rural Development of China, *Code for Seismic Design of Buildings, GB 50011-2010*, Ministry of Housing and Urban-Rural Development, Beijing, China, 2010, in Chinese.

[22] Research Center for Cold-Formed Steel Structures at Chang'an University (CFS-CHD), *Shear Performance of Cold-Formed Thin-Walled Shear Walls, No. 2004-01*, Chang'an University, Xi'an, China, 2004, in Chinese.

[23] Research Center for Cold-Formed Steel Structures at Chang'an University (CFS-CHD), *Experimental Research on Shear Behavior of Q550 High Strength Cold-Formed Steel Framing Walls, No. 2009-01*, Chang'an University, Xi'an, China, 2009, in Chinese.

[24] Research Center for Cold-Formed Steel Structures at Chang'an University (CFS-CHD), *Cyclic Loading Tests on Cold-Formed Steel Framing Walls with Infilled Lightweight FGD Gypsum, No. 2017-02*, Chang'an University, Xi'an, China, 2017, in Chinese.

[25] American Iron and Steel Institute (AISI), *North American Standard for Cold-Formed Steel Framing-Lateral Design, AISI S213*, American Iron and Steel Institute (AISI), Washington, DC, USA, 2007.

[26] K. N. Li, "CANNY-C–a computer program for 3D nonlinear dynamic analysis of building structures," Research Report No. CE004, Department of Civil Engineering, National University of Singapore, Singapore, 1993.

[27] Z. G. Huang, M. Z. Su, B. K. He et al., "Shaking table test on seismic behaviors of three-story cold-formed thin-wall steel residential buildings," *China Civil Engineering Journal*, vol. 44, no. 2, pp. 73–81, 2011, in Chinese.

[28] F. Liu, Y. Q. Li, and Z. Y. Shen, "Shaking table test investigation on a full-scale high-strength cold-formed thin-walled steel residential building," in *Proceedings of the 9th international conference on steel, space & composite structures*, Beijing, China, Oct 2007.

[29] Y. Shi, X. H. Zhou, L. P. Liu et al., "Shaking table test on prefabricated light steel structure popular science building," *Journal of Building Structures*, vol. 40, no. 2, pp. 98–107, 2019, in Chinese.

[30] China Engineering Construction Association Standard, *Code for Anti-Collapse Design of Building Structures, CECS 392-2014*, Beijing, China, 2014, in Chinese.

[31] H. Hwang and J. W. Jaw, "Statistical evaluation of deflection amplification factors for reinforced concrete structures," in *Proceedings of the Fourth U.S. National Conference on Earthquake Engineering*, vol. 937–944, Palm Springs, California, May 1990.

[32] J. I. Baez and E. Miranda, "Amplification factors to estimate inelastic displacement demands for the design of structures in the near field," in *Proceedings of the 12th World Conference on Earthquake Engineering*, Auckland, New Zealand, January 2000.